Journal of Pharmaceutical Analysis 12 (2022) 570–582

Contents lists available at ScienceDirect

Journal of Pharmaceutical Analysis

journal homepage: www.elsevier.com/locate/jpa

Original article

18beta-glycyrrhetinic acid induces ROS-mediated apoptosis to ameliorate hepatic fibrosis by targeting PRDX1/2 in activated HSCs

Qian Zhang [a, c, 1], Piao Luo [a, c, 1], Liuhai Zheng [c], Jiayun Chen [a], Junzhe Zhang [a], Huan Tang [a], Dandan Liu [a], Xueling He [a], Qiaoli Shi [a], Liwei Gu [a], Jiahao Li [a], Qiuyan Guo [a], Chuanbin Yang [c], Yin Kwan Wong [b], Fei Xia [a, *], Jigang Wang [a, **]

[a] Artemisinin Research Center and Institute of Chinese Materia Medica, Chinese Academy of Chinese Medical Sciences, Beijing, 100700, China
[b] Department of Biological Sciences, National University of Singapore, Singapore, 117543, Singapore
[c] Department of Geriatrics, Shenzhen People's Hospital (The Second Clinical Medical College, Jinan University), Shenzhen, 518020, China

ARTICLE INFO

Article history:
Received 15 December 2021
Received in revised form
31 May 2022
Accepted 1 June 2022
Available online 8 June 2022

Keywords:
Glycyrrhetinic acid
Hepatic fibrosis
Peroxiredoxin
Reactive oxygen species
Apoptosis

ABSTRACT

Hepatic stellate cells (HSCs) are essential drivers of fibrogenesis. Inducing activated-HSC apoptosis is a promising strategy for treating hepatic fibrosis. 18beta-glycyrrhetinic acid (18β-GA) is a natural compound that exists widely in herbal medicines, such as *Glycyrrhiza uralensis* Fisch, which is used for treating multiple liver diseases, especially in Asia. In the present study, we demonstrated that 18β-GA decreased hepatic fibrosis by inducing the apoptosis in activated HSCs. 18β-GA inhibited the expression of α-smooth muscle actin and collagen type I alpha-1. Using a chemoproteomic approach derived from activity-based protein profiling, together with cellular thermal shift assay and surface plasmon resonance, we found that 18β-GA covalently targeted peroxiredoxin 1 (PRDX1) and peroxiredoxin 2 (PRDX2) proteins via binding to active cysteine residues and thereby inhibited their enzymatic activities. 18β-GA induced the elevation of reactive oxygen species (ROS), resulting in the apoptosis of activated HSCs. *PRDX1* knockdown also led to ROS-mediated apoptosis in activated HSCs. Collectively, our findings revealed the target proteins and molecular mechanisms of 18β-GA in ameliorating hepatic fibrosis, highlighting the future development of 18β-GA as a novel therapeutic drug for hepatic fibrosis.

1. Introduction

Hepatic fibrosis, a long-term hepatic disease characterized by overproduction of extracellular matrix (ECM), is a fundamental public health threat worldwide and can be a consequence of viral hepatitis, alcoholic hepatitis, nonalcoholic steatohepatitis, or cholestatic diseases [1]. Hepatic fibrosis is a key pathological stage that induces liver failure in conditions such as cirrhosis and carcinoma [2]. Although the exact mechanisms of the pathogenesis of hepatic fibrosis are still unclear, hepatic stellate cells (HSCs) are currently regarded as one of the crucial players promoting the development of hepatic fibrosis by inducing the deposition of ECM [3]. Targeting HSCs has gradually been considered as an essential approach for hepatic fibrosis treatment, which mainly includes inhibiting the activation of HSCs, inducing the apoptosis of HSCs, and regulating the synthesis and degradation of collagen [4,5]. Previous studies have shown promoting the death of activated-HSC ameliorates the pathological development of hepatic fibrosis [6,7]. Thus, inducing apoptosis in HSCs is an essential approach for the treatment of fibrosis [8].

Mitochondria are indispensable organelles involved in cell differentiation, apoptosis, growth, and energy metabolism [9]. Mitochondrial dysfunction and structural damage may cause abnormal energy metabolism and overproduction of reactive oxygen species (ROS) [10]. ROS play a dual role in the pathogenesis of hepatic fibrosis [11,12]. Emerging evidence has shown that ROS-mediated apoptosis is a novel strategy for fibrosis treatment in activated HSCs [13]. In addition, emerging studies have indicated that the induction of mitochondria-mediated apoptosis in activated HSCs can effectively attenuate hepatic fibrosis [14–16]. Overall, inducing the ROS-associated apoptosis in activated HSCs may contribute to their clearance for further clinical treatment of hepatic fibrosis.

Peer review under responsibility of Xi'an Jiaotong University.
* Corresponding author.
** Corresponding author.
E-mail addresses: fxia@icmm.ac.cn (F. Xia), jgwang@icmm.ac.cn (J. Wang).
[1] Both authors contributed equally to this work.

https://doi.org/10.1016/j.jpha.2022.06.001

18beta-glycyrrhetinic acid (18β-GA) is an active metabolite of glycyrrhizic acid obtained from Chinese herbal licorice root (Fig. 1A). Herbal plants are popularly used as herbal medicines for treating various tumors, inflammation, and viral infections [17–20]. Notably, 18β-GA protects against viral hepatitis, hepatic fibrosis and injury, and hepatocellular carcinoma [21–23]. To date, 18β-GA has been known to exert its hepatoprotective effects mainly through antiviral, anti-inflammatory, and antioxidant activities; however, the mechanisms of action and target proteins of 18β-GA remain elusive.

In the present study, it was shown that 18β-GA ameliorated bile duct ligation (BDL)-induced liver damage and fibrosis by inducing apoptosis in activated HSCs. Activity-based protein profiling (ABPP) in combination with the cellular thermal shift assay (CETSA) approach showed that 18β-GA covalently bound to peroxiredoxin 1 (PRDX1) and peroxiredoxin 2 (PRDX2) and inhibited their antioxidant activity, which eventually triggered oxidative stress and led to apoptosis. Collectively, these findings revealed a ROS-mediated mechanism of 18β-GA for the treatment of hepatic fibrosis by targeting PRDX1/PRDX2.

2. Methods

2.1. Reagents and materials

18β-GA was obtained from J&K Scientific (Shanghai, China). Platelet-derived growth factor-beta polypeptide and *N*-acetyl-L-cysteine (NAC) were purchased from AbMole BioScience (Shanghai, China). The cell apoptosis detection kit was purchased from BD Biosciences (Franklin Lake, NJ, USA). Specific primary antibodies used were as follows: alpha-smooth muscle actin (α-SMA), PRDX1, PRDX2 (Abcam, Cambridge, UK), collagen type I alpha-1 (COL1α1), and vimentin (VIM) (Proteintech, Chicago, IL, USA). β-actin antibody was obtained from Affinity Biosciences (Changzhou, China).

2.2. Synthesis of probes

2.2.1. 18β-GA probe 1 (P1)

A mixture of 18β-GA (141 mg, 0.30 mmol), *O*-(7-azabenzotriazol-1-yl)-*N*,*N*,*N*′,*N*′-tetramethyluronium hexafluorophosphate (171 mg, 0.45 mmol), Et_3N (90.9 mg, 0.90 mmol), and monopropargylamine (16.5 mg, 0.30 mmol) in *N*,*N*-dimethylformamide (DMF, 3 mL) was stirred at room temperature. The reaction mixture was diluted with ddH_2O (3 mL) and extracted with ethyl acetate (20 mL for twice). Subsequently, the organic phases were combined, washed with brine (5 mL for thrice), dried over anhydrous Na_2SO_4, and concentrated. The sample was further purified using flash column chromatography to obtain the final product, P1. White solid (yield: 72%); ^{1}H NMR (600 MHz, $CDCl_3$) δ 5.79 (s, 1H), 5.69 (s, 1H), 4.01–4.12 (m, 2H), 3.22–3.23 (m, 1H), 2.96 (s, 1H), 2.88 (s, 1H), 2.79 (d, J = 12 Hz, 1H), 2.34 (s, 1H), 2.25 (s, 1H), 2.15–2.17 (m, 1H), 2.02–2.06 (m, 1H), 1.94 (d, J = 12 Hz, 1H), 1.84 (t, J = 24 Hz, J = 12 Hz, 1H), 1.72–1.76 (m, 2H), 1.59–1.65 (m, 5H), 1.37–1.48 (m, 8H), 1.14 (d, J = 6 Hz, 9H), 0.95–1.04 (m, 5H), 0.82 (d, J = 6 Hz, 6H); ^{13}C NMR (125 MHz, $CDCl_3$) δ 200.2, 175.5, 169.0, 128.6, 79.7, 78.8, 71.7, 61.9, 55.0, 48.0, 45.4, 43.6, 43.2, 41.9, 39.2, 39.1, 37.1, 31.9, 29.3, 28.4, 28.1, 27.3, 26.5, 26.4, 23.4, 18.7, 16.4, and 15.6; high-resolution mass spectrometry (HRMS) *m/z*: $[M+H]^+$ calculated for $C_{33}H_{50}NO_3$ 508.3785 and found 508.3770.

2.2.2. 18β-GA probe 2 (P2)

A mixture of 18β-GA (141 mg, 0.30 mmol), K_2CO_3 (49.68 mg, 0.36 mmol), 18-crown-6 (7.93 mg, 0.03 mmol), and 5-chloro-1-pentyne (36.92 mmol, 0.36 mmol) in acetonitrile (MeCN, 3 mL) was refluxed overnight in N_2. The suspension was filtered and concentrated. The sample was purified using flash column chromatography to obtain the final product, P2. White solid (yield: 54%); ^{1}H NMR (600 MHz, $CDCl_3$) δ 5.64 (s, 1H), 4.20 (s, 2H), 3.22 (d, J = 6 Hz, 1H), 2.79 (d, J = 12 Hz, 1H), 2.34 (s, 1H), 2.30 (s, 2H), 2.10 (d, J = 12 Hz, 1H), 1.98–2.04 (m, 3H), 1.81–1.92 (m, 4H), 1.59–1.67 (m, 6H), 1.39–1.47 (m, 2H), 1.36 (s, 3H), 1.25–1.33 (m, 4H), 1.08–1.19 (m, 10H), 0.95–1.02 (m, 5H), 0.80 (s, 6H); ^{13}C NMR (125 MHz, $CDCl_3$) δ 200.2, 176.3, 169.1, 128.6, 82.7, 78.8, 69.3, 62.9, 61.8, 55.0, 48.4, 45.4, 44.0, 43.2, 41.1, 39.1, 37.8, 37.1, 32.8, 31.9, 31.1, 28.6, 28.4, 28.1, 27.5, 27.3, 26.5, 26.4, 23.4, 18.7, 17.5, 16.4, 15.6, and 15.3; HRMS *m/z*: $[M+H]^+$ calculated for $C_{35}H_{53}O_4$ 537.3938 and found 537.3922.

2.3. Cell culture and cell counting kit (CCK-8) assays

Human HSC line (LX-2) and mouse HSCs (mHSCs) were cultured in Dulbecco's Modified Eagle Medium supplemented with 10% fetal bovine serum, penicillin, and streptomycin (Gibco, Foster, CA, USA) at 37 °C, with 5% CO_2 in a 95% humidified atmosphere. To measure the viability of cells following treatment with 18β-GA, P1, P2, or NAC, the CCK-8 (Dojindo, Kyushu, Japan) was used.

2.4. Experimental models of fibrotic mice

The hepatic fibrosis model was established in C57BL/6 male mice (21 ± 2 g) using BDL [24,25]. Animal experiments were approved by the China Animal Care and Use Committee and were conducted in accordance with Regulations on the Care and Use of the Laboratory Animal Center of Shenzhen People's Hospital. The mice were divided into four groups (8 mice per group). The control group did not undergo BDL or receive 18β-GA; the BDL model group underwent BDL; and the 18β-GA-25 and 18β-GA-50 groups underwent BDL, followed 24 h later by gavage with 18β-GA. The mice were administered 18β-GA (25 or 50 mg/kg) once daily for 12 days. All mice were anesthetized to collect serum and liver samples.

2.5. Biochemical and histological assays

Alanine aminotransferase (ALT), direct bilirubin (DBil), aspartate transaminase (AST), and total bilirubin (TBil) levels were detected in the serum. The kits were purchased from Beijian Xinchuangyuan Technology (Beijing, China). Liver tissues were fixed, embedded, sectioned, stained with hematoxylin and eosin (H&E) for histological examination, and stained with Sirius red and masson. Liver tissue samples were examined under a light microscope (3DHIESTECH, Budapest, Hungary) for each microscopic field.

2.6. Western blot analysis

Total proteins were extracted from samples, followed by electrophoresis with 10% sodium dodecyl sulfate-polyacrylamide gel electrophoresis (SDS-PAGE), electro-transferred, and then treated with primary and secondary antibodies. Bands were visualized using enzyme-linked chemiluminescence (Thermo Fisher, Waltham, MA, USA), and signals were analyzed using ImageJ software.

2.7. Flow cytometry

Cells were seeded in 24-well plates with or without 18β-GA treatment. After collecting the cells, they were gently washed, resuspended in 1× binding buffer, and added to 5 μL of annexin-fluorescein isothiocyanate and 5 μL of propidium iodide. Cells were then incubated for 10 min in the dark and analyzed using flow cytometry.

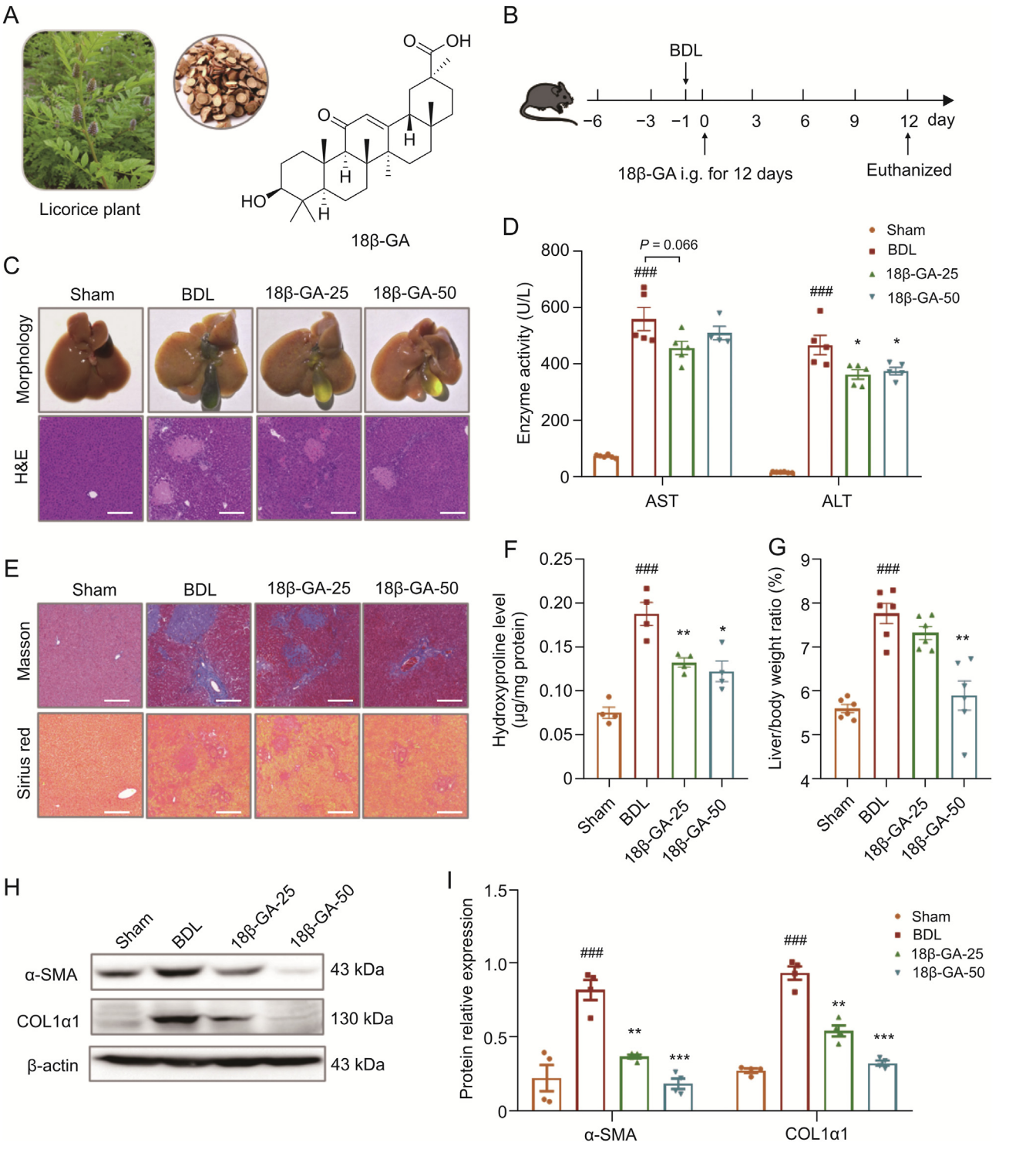

Fig. 1. 18beta-glycyrrhetinic acid (18β-GA) exerts anti-fibrosis effects on bile duct ligation (BDL)-induced fibrotic mice. (A) Licorice plant, decoction pieces and structure of 18β-GA. (B) Experimental scheme of animal in this study. Grouping was as follows: Sham; BDL; 18β-GA-25 and 18β-GA-50 groups underwent BDL, followed by gavage 18β-GA (25 and 50 mg/kg). (C) Representative photographs of the liver and hematoxylin and eosin (H&E) of histological examination (scale bar = 200 μm). (D) Effects of 18β-GA on the serum alanine aminotransferase and aspartate transaminase in mice ($n = 5$). (E) Liver sections with collagen deposition staining (scale bar = 50 μm). (F) Measurement of hydroxyproline level in fibrotic liver of mice ($n = 4$). (G) Ratios of liver/body weight in mice ($n = 6$). (H) Anti-fibrosis effect of 18β-GA for expressions of alpha smooth muscle actin (α-SMA), and collagen type I alpha-1 (COL1α1) in mice. (I) Analyses of proteins with densitometry corresponding to Fig. 1H ($n = 4$). Mean ± SEM, $^{\#\#}P < 0.01$, $^{\#\#\#}P < 0.001$ vs. Sham; $^{*}P < 0.05$, $^{**}P < 0.01$, $^{***}P < 0.001$ vs. BDL Model.

2.8. Fluorescence imaging

Cells were treated with P1, fixed, and permeabilized. P1 was conjugated with using click chemistry. Subsequently, the cells were incubated with primary antibodies, secondary fluorescent antibodies, and Hoechst dye. Cellular images were obtained using a laser scanning confocal fluorescence microscope (Leica, Hamburg, Germany). JC-1 (BD Biosciences, Franklin Lake, NJ, USA) staining was also performed.

2.9. Measurement of ROS

The cells were incubated with 18β-GA. ROS levels were measured as previously described [26] using a CM-H2DCF-DA kit (Jiancheng Bioengineering, Nanjing, China).

2.10. Pull-down assay and liquid chromatography tandem-mass spectrometry (LC-MS/MS)

To identify the cellular target protein of 18β-GA, pull-down experiments were performed, followed by in situ Western blotting. The experimental procedures were similar to those described previously [27]. The cells were incubated with or without competitors before P1. After incubation for another 4 h, the cells were collected. A soluble protein solution was extracted, and a click chemistry reaction cocktail was added to the solution as described above before precipitation with pre-chilled acetone (−20 °C). The protein was dissolved in phosphate buffer saline (PBS) containing 1.5% SDS before incubation with beads. Subsequently, the beads were washed with 1% SDS in PBS, 0.1% SDS in PBS, and 6 M urea in PBS, respectively. Beads were enriched with protein and then separated using SDS-PAGE, followed by detection using western blotting. For the identification of target proteins using LC-MS/MS [28], the specific molecular weight bands were excised and washed, and the samples were reduced and alkylated using dithiothreitol and iodoacetamide, respectively. Subsequently, proteins were digested into peptides using trypsin. Finally, the peptides were analyzed using LC-MS/MS.

2.11. CETSA

To further confirm the 18β-GA targeted proteins, a CETSA-Western blot experiment was implemented similarly to previously described [29]. LX-2 cells were lysed with PBS buffer with 1 mM protease inhibitor cocktail. The lysates were incubated with 18β-GA (50 μM) for 1 h at room temperature. Equal amounts of proteins were aliquoted into tubes, and then heated at different temperatures 37–73 °C. After centrifugation, the soluble supernatants in samples were treated with a loading buffer, followed by Western blot analysis.

2.12. Plasmids and protein purification

Human *PRDX1* (GenBank accession No.: NP_859048.1), cysteine-mutated *PRDX1* (Cys52Ser), and *PRDX2* (GenBank accession No.: NP_005800.3) were subcloned into the pET28a vector (Sangon, Shanghai, China) to generate proteins. *Escherichia coli* strain BL21 was transformed with pET28a-*PRDX1* and cysteine-mutated plasmids in Luria-Bertani medium and induced to express proteins by 0.4 mM isopropyl-D-1-thiogalactopyranoside. Bacterial pellets were collected and lysed with binding buffer. The supernatants containing His-tagged recombinant *PRDX1*, *PRDX2*, and the mutated variants were harvested using centrifugation at 12,000 r/min for 5 min. Proteins were purified using an Ni-bead column (QIAGEN, Valencia, CA, USA). The Ni-bead column was eluted with recombinant proteins and purified using an Ni-NTA bead column. Imidazole in the samples was buffer-exchanged, and samples were concentrated. The purity and integrity of the recombinant protein were visualized using Coomassie Brilliant Blue staining.

2.13. Surface plasmon resonance (SPR)

An SPR assay was carried out to investigate the binding kinetics using the Biacore T200 system (Biacore, GE Healthcare, Stockholm, Sweden). The experimental procedures were similar to those previously described [30]. 18β-GA was immobilized on the surface of the sensor chip at 30 μL/min for 1 min, followed by 2 min of dissociation. The SPR results were analyzed using Biacore evaluation software.

2.14. Molecular docking model

PRDX1 (PDB: 4XCS) and PRDX2 (PDB: 1QMV) were obtained from Protein Data Bank (PDB). Discovery Studio client software was used for hydrogenation and dehydration. Subsequently, PyMOL and Pyrx-0.8 software were used for docking and mapping, respectively.

2.15. Activity assay

Antioxidant activity was monitored as previously described [31,32]. Briefly, rhPRDX1 was incubated with 18β-GA in 96-well plates. The PRDX1 activity was determined using a hydrogen peroxide kit (Shanghai, China).

2.16. Transfection assay

Small interfering RNAs (Table S1) were modified with carboxyfluorescein to determine the transfection efficiency. These vectors were co-transfected with packaging plasmids using lipofectamine 2000 (Invitrogen, Waltham, MA, USA) into LX-2 cells. Apoptotic cells were measured using flow cytometry from the transfected cell samples.

2.17. Statistical analysis

Data are shown as mean ± SEM. Experimental data from several groups were analyzed using one-way ANOVA and Tukey's test. Both groups were analyzed using unpaired two-tailed *t*-tests. All data were analyzed using GraphPad Prism software (version 8.0).

3. Results

3.1. 18β-GA mitigated BDL-induced hepatic fibrosis in mice

The antifibrotic effect of 18β-GA was first evaluated on a hepatic fibrosis mouse model using BDL. After BDL, mice were administered vehicle or 18β-GA using gavage for 12 days (Fig. 1B). Our data indicated that 18β-GA exerted a significant inhibitory effect on liver injury and fibrosis in BDL-induced mice, and reduced cholestasis, the infiltration of inflammatory cells, and hemorrhagic necrosis (Fig. 1C), decreased the liver/body weight ratio (Fig. 1G), as well as levels of ALT, AST, TBil, and DBil in serum (Figs. 1D, S1A, and S1B). To further investigate the inhibition of hepatic fibrosis, fibrosis-related indices were assessed. 18β-GA treatment markedly decreased ECM deposition (Fig. 1E). The hydroxyproline test further supported the observation that collagen overproduction was abolished after 18β-GA treatment (Fig. 1F). Moreover, 18β-GA inhibited the expression of α-SMA (a marker for activated HSCs), COL1α1, and VIM (a marker for HSCs activation) in vivo (Figs. 1H, 1I, S1C, and S1D). These results suggest that 18β-GA improved BDL-induced hepatic fibrosis.

3.2. 18β-GA suppressed hepatic fibrosis by inducing activated-HSC apoptosis

Next, the underlying mechanisms of 18β-GA in activated HSCs were explored. The data indicated that α-SMA and COLIα1 expressions were significantly increased in activated mHSCs compared to non-activated cells, while 18β-GA decreased the expressions of fibrosis biomarkers (α-SMA and COLIα1 proteins) in activated mHSCs (Figs. 2A and B) and LX-2 cells (Figs. S2A and B).

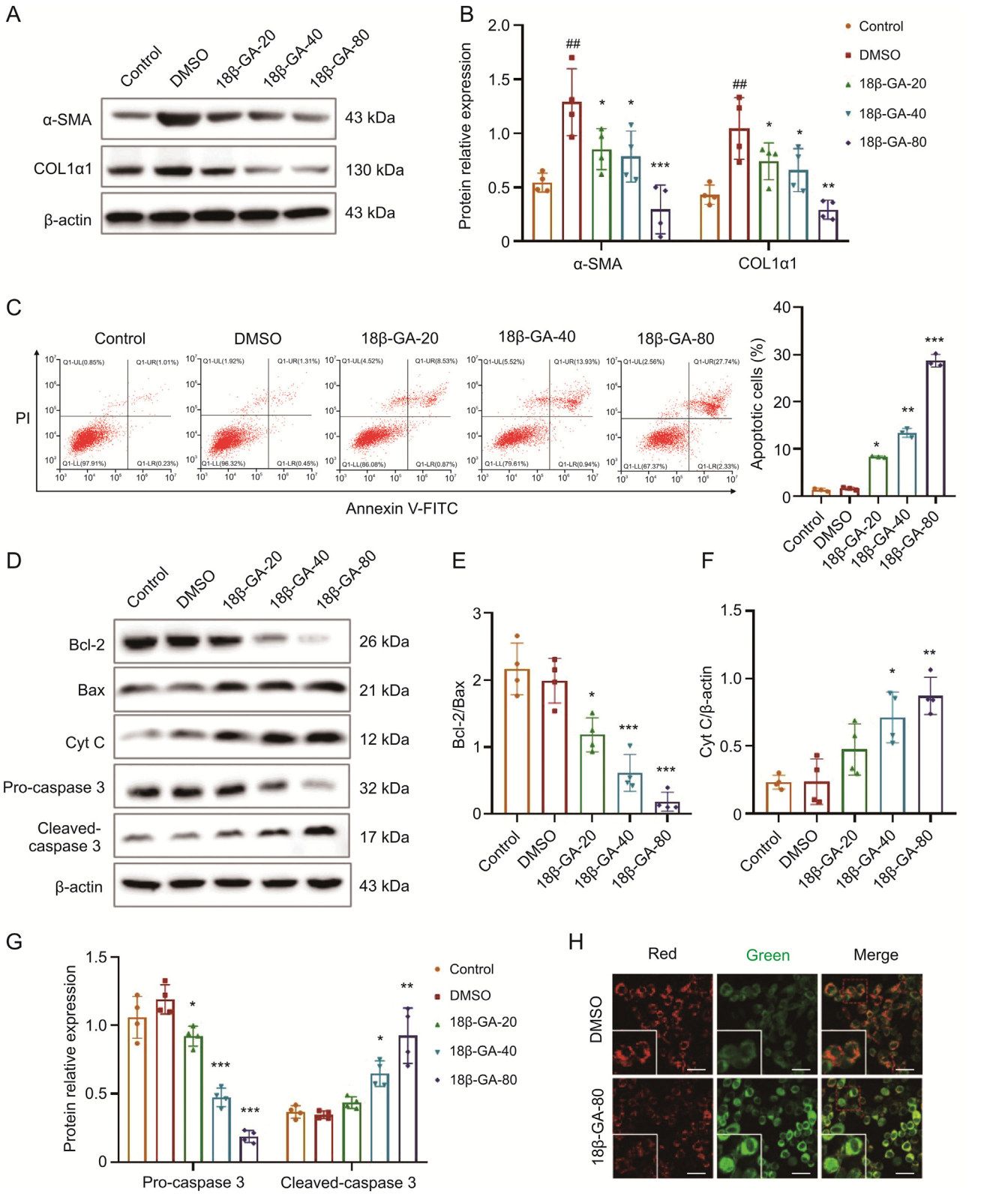

Fig. 2. 18β-GA induced apoptosis of activated mouse hepatic stellate cells (mHSCs). Grouping was as follows: control (quiescent cells); DMSO (20 ng/mL PDGF-BB); 18β-GA-20, 18β-GA-40, and 18β-GA-80 groups were treated with 20 ng/mL PDGF-BB, followed by 18β-GA (20, 40, and 80 μM). (A) The anti-fibrosis effect of 18β-GA on the α-SMA and COL1α1 expressions in activated mHSCs. (B) Western blot analyses with densitometry corresponding to Fig. 2A ($n = 4$) in mHSCs. (C) Percentage of apoptotic cells by flow cytometry ($n = 3$). (D) Changes in apoptosis-related proteins induced by 18β-GA in mHSCs. (E–G) Analyses of proteins with densitometry corresponding to Fig. 2D ($n = 4$). (H) Fluorescence imaging of JC-1 staining of mitochondria in mHSC cells by 18β-GA (80 μM) (scale bar = 30 μm). Mean ± SEM, $^{*}P < 0.05$, $^{**}P < 0.01$, $^{***}P < 0$ 0.01, vs. DMSO; $^{\#\#}P < 0.01$ vs. control. Cyt C: cytochrome C; PI: propidium iodide; FITC: fluoresceine isothiocyanate; DMSO: dimethyl sulfoxide; PDGF-BB: platelet-derived growth factor beta polypeptide.

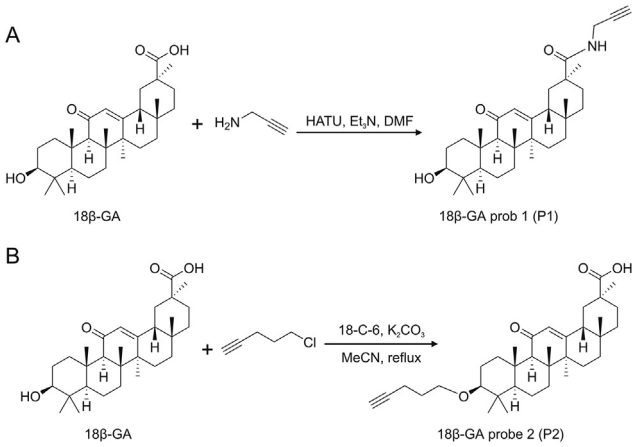

Scheme 1. Synthesis routes of two 18β-GA probes. (A) Structures of 18β-GA and the alkyne-tagged-clickable probe 1 (P1) and (B) 18β-GA alkyne-tagged-clickable probe 2 (P2). HATU: hexafluorophosphate; Et3N: triethylamine; DMF: dimethylformamide; MeCN: acetonitrile.

Then, the effect of 18β-GA on apoptotic cells was explored. 18β-GA contributed to cell apoptosis, and the percentage of apoptotic cells was increased by 18β-GA in activated mHSCs (Fig. 2C) and LX-2 cells (Fig. S2C). The mechanism of apoptosis in the cells was explored. The results showed that the effect of 18β-GA on the ratio of B-cell lymphoma 2/Bcl-2 associated X (Bcl-2/Bax) was significantly decreased, while caspase activation and cytochrome C (Cyt C) release were markedly increased by 18β-GA in activated mHSCs (Figs. 2D–G) and LX-2 cells (Figs. S2D–H). Furthermore, the mitochondrial membrane potential detection probe JC-1, which displays green fluorescence in damaged mitochondria, was used. The results showed that 18β-GA caused mitochondrial damage in mHSC cells (Fig. 2H). The above results suggested that 18β-GA induced the apoptosis of activated-HSC, possibly through inducing mitochondrial dysfunction.

Table 1
The selected differentially enriched proteins.

Proteins	Molecular weight (kDa)	Coverage (%)	Peptides	Protein abundance ratio [a]
★ HSPA5	72.3	20	11	1.3168
★ CCT6A	58	14	6	2.4559
★ VDAC	31.5	15	4	1.4579
★ PRDX1	22	25	5	2.0562
★ PRDX2	22	20	4	1.4966

[a] Protein abundance ratio represents the protein abundance identified by LC-MS/MS between probe group and dimethyl sulfoxide (control) group; "★" Representative target proteins corresponding to "★" label protein bands in Fig. 3C. HSPA5: heat shock protein A5; CCT6A: chaperonin containing TCP1 subunit 6A; VDAC: voltage-dependent anion channel; PRDX: peroxiredoxin.

3.3. Identification of 18β-GA target proteins using ABPP

To explore the direct binding proteins of 18β-GA and how 18β-GA induces apoptosis, two alkyne-tagged 18β-GA probes (P1 and P2) were designed and synthesized (Scheme 1). The structures of P1 (Figs. S3–S5) and P2 (Figs. S6–S8) were further validated using ^{1}H NMR, ^{13}C NMR, and high-resolution mass spectrometry (HRMS).

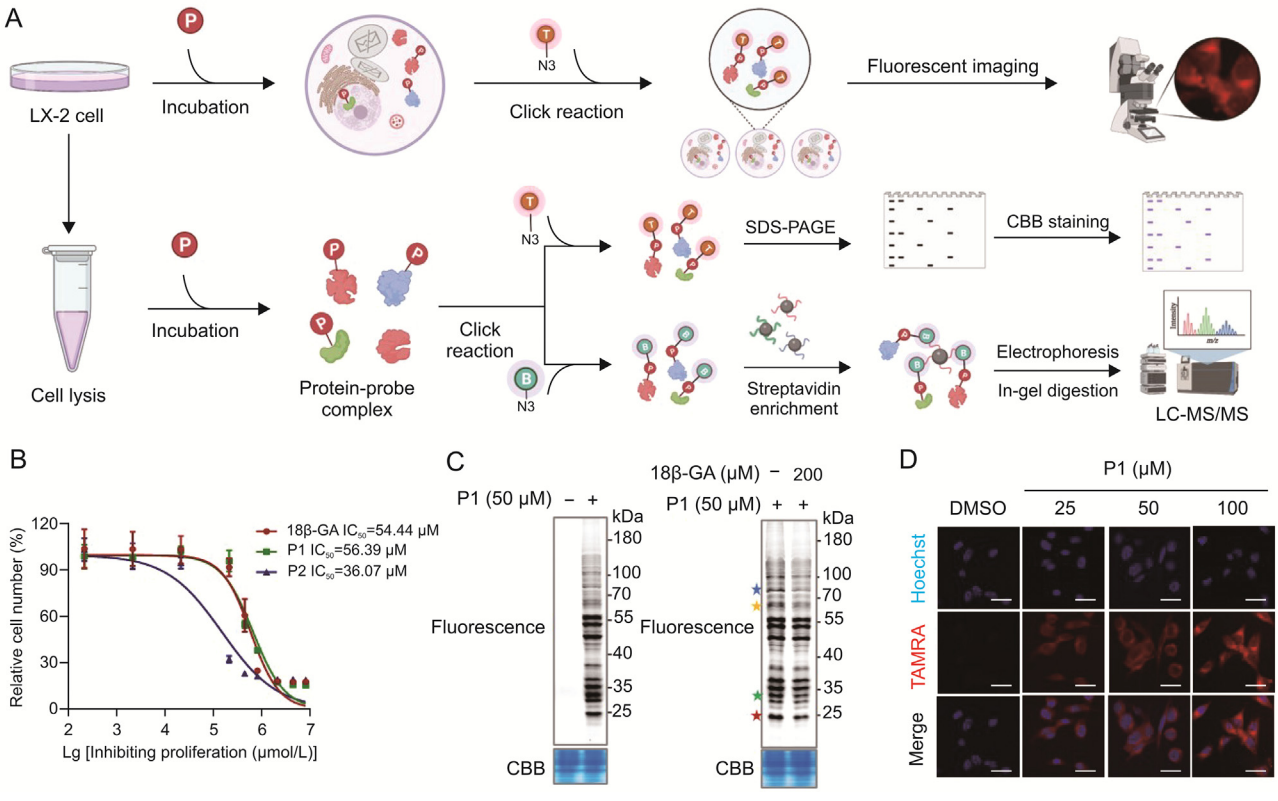

Fig. 3. Identification of 18β-GA target proteins. (A) Schematic model of activity-based protein profiling (ABPP) to profile potential 18β-GA protein targets. (B) Inhibiting proliferation in LX-2 cells by 18β-GA and 18β-GA probes ($n = 3$). (C) Labeling or competition assay of P1 in LX-2 cell lysates. (D) Cellular imaging of P1 in LX-2 cells (scale bar = 25 μm). SDS-PAGE: sulfate-polyacrylamide gel electrophoresis; CBB: Coomassie Brilliant Blue; LC-MS/MS: liquid chromatography tandem-mass spectrometry.

Next, a chemical proteomics strategy was used to identify the target proteins of 18β-GA, as illustrated in Fig. 3A. First, the inhibitory effect of the probes on LX-2 cells was evaluated. The results showed that P1 possessed the similar potent biological activity as that of 18β-GA (Fig. 3B). Subsequently, the two probes were incubated in cell lysates and then attached to a fluorescent dye to label the target proteins. Results showed that P1 had a higher fluorescence intensity than P2 (Fig. S9); thus, P1 was chosen for further target identification experiments. Notably, the labeling assay indicated that several bands were observed at approximately 70, 58, 30, and 25 kDa, and fluorescence significantly diminished after pretreatment with 18β-GA (Fig. 3C). Cellular imaging experiments were performed, and P1 labeling was observed in the cytoplasm and nucleus of the cells (Fig. 3D). Thus, these bands were excised, followed by in-gel tryptic digestion and protein identification using LC-MS/MS. Several representative target proteins were highlighted from the list of identified proteins, including PRDX1 and PRDX2 (Table 1). These results suggested that PRDX1/PRDX2 were direct binding protein targets of 18β-GA. Therefore, PRDX1 and PRDX2 were focused in subsequent analyses.

3.4. 18β-GA directly targeted PRDX1 and PRDX2

To further confirm the direct binding of 18β-GA to PRDX1 and PRDX2, pull-downs followed by immunoblotting assays were performed. The results showed that P1 could bind to PRDX1 and

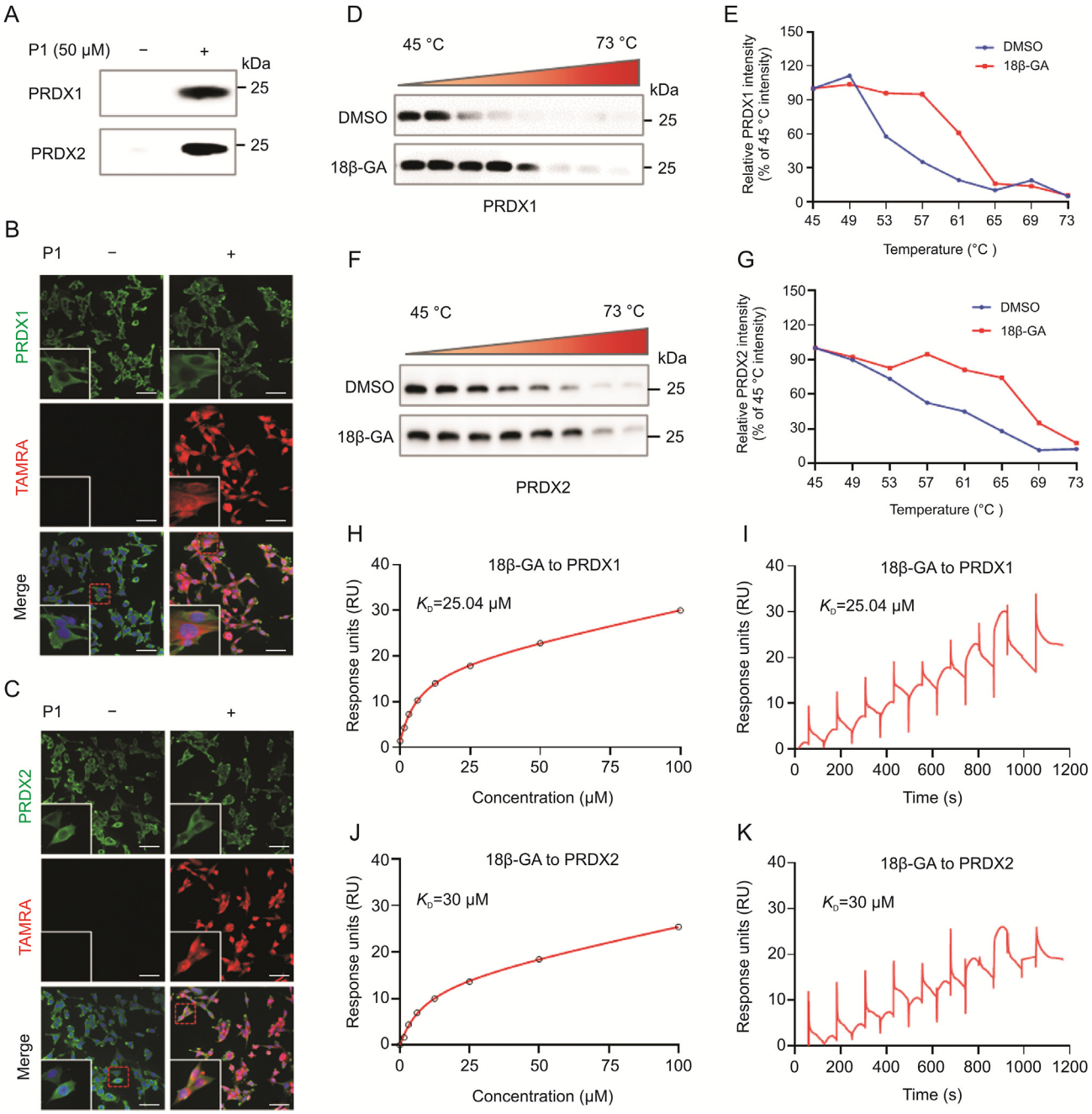

Fig. 4. 18β-GA directly targeted peroxiredoxin 1 (PRDX1) and PRDX2. (A) Pull down-Western blot to verify that 18β-GA directly targets PRDX1 and PRDX2 proteins. (B and C) Immunofluorescence staining of PRDX1 and PRDX2 (green) and P1 clicked with TAMRA (red), scale bar = 75 μm. (D–G) Cellular thermal shift assay (CETSA)-Western blot to test the interactions of 18β-GA and PRDX1 or PRDX2. (H–K) Surface plasmon resonance experiments to assess the binding kinetics between 18β-GA and PRDX1 or PRDX2 proteins.

PRDX2 proteins (Fig. 4A). The colocalization of P1 with PRDX1 and PRDX2 was also visualized using immunofluorescence staining (Figs. 4B and C). When target proteins bind to small molecules, they often become thermostable. Thus, a CETSA assay was performed to detect the binding efficiency between proteins and small molecules by evaluating the thermostability of target proteins [33]. The results indicated that thermal stability of both PRDX1 and PRDX2 was increased compared to the DMSO group, which supported these two proteins as direct binding targets of 18β-GA (Figs. 4D–G). In addition, an SPR assay was carried out to investigate the dynamic

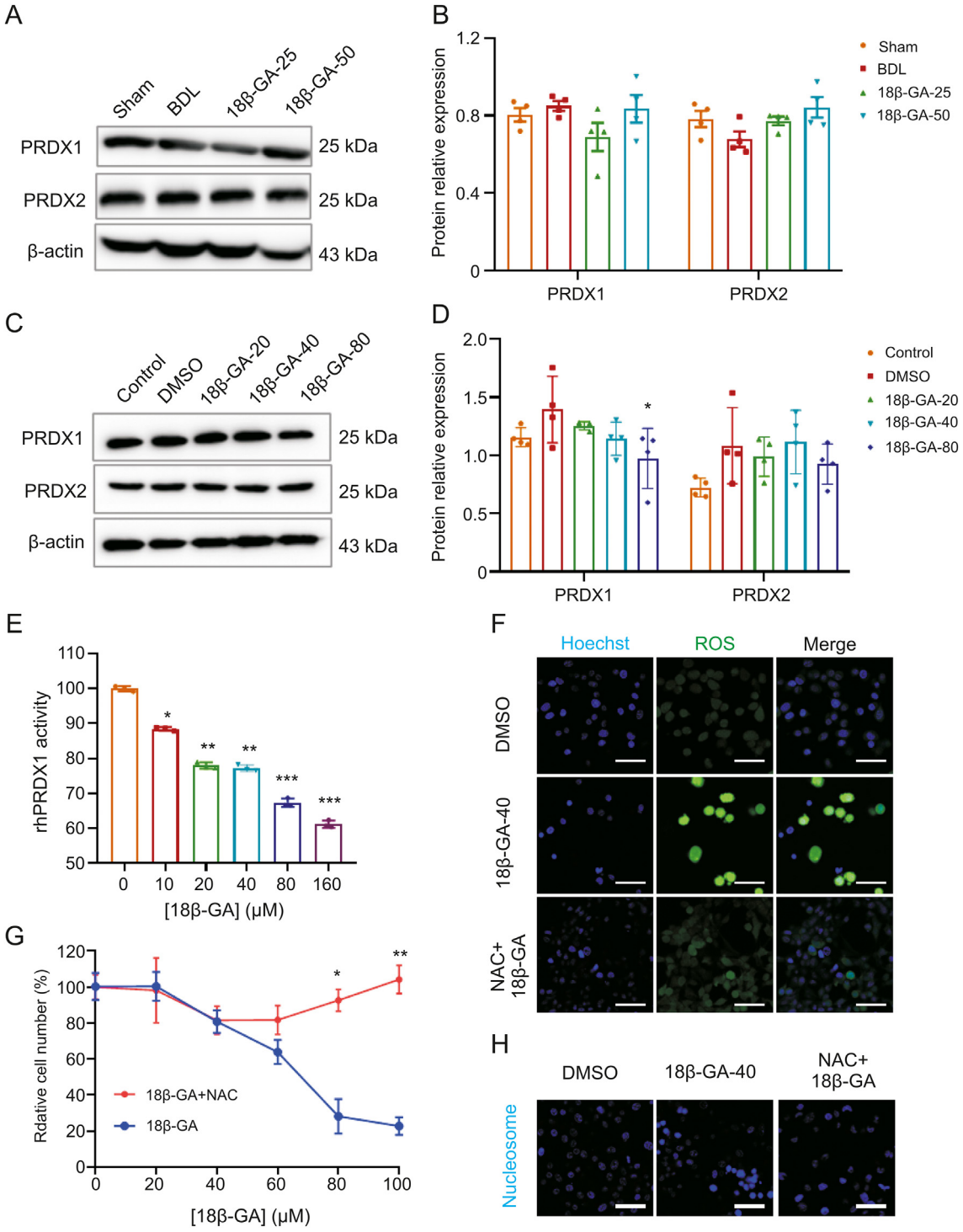

Fig. 5. 18β-GA inhibited antioxidant activities of target proteins. (A) Expressions of PRDX1 and PRDX2 in the liver tissue of BDL-induced mice by 18β-GA. (B) Western blot analyses of protein with densitometry corresponding to Fig. 5A ($n = 4$). (C) Expression levels of PRDX1 and PRDX2 in mHSCs by 18β-GA. (D) Western blot analyses of protein with densitometry corresponding to Fig. 5C ($n = 4$). (E) Catalytic activity of recombinant human PRDX1 (rhPRDX1) protein was measured by detecting residual H_2O_2 levels ($n = 3$). (F) Cellular reactive oxygen species (ROS) staining (green) in LX-2 cells, scale bar = 50 μm. (G) Viabilities of LX-2 cells treatment with 18β-GA or co-treatment with *N*-acetyl-L-cysteine (NAC) ($n = 3$). (H) Intracellular nucleosome staining after treatment with 18β-GA (40 μM) and NAC (200 μM) in LX-2 cells (scale bar = 50 μm). Mean ± SEM, $^{*}P < 0.05$, $^{**}P < 0.01$, $^{***}P < 0.001$ vs. DMSO or Sham.

properties of 18β-GA and the two targets. The results showed a remarkable binding between 18β-GA and PRDX1 or PRDX2, with K_D values of 25.04 and 30 μM, respectively (Figs. 4H–K). These results suggested that 18β-GA directly bound to PRDX1 and PRDX2.

3.5. 18β-GA inhibited enzymatical activities of target proteins

The expression levels of PRDX1 and PRDX2 were also measured. The results indicated that 18β-GA did not affect the expressions of PRDX1 and PRDX2 in BDL-induced fibrotic liver tissue (Figs. 5A and B). However, 18β-GA (80 μM) slightly down-regulated the expression of PRDX1, but not PRDX2 in activated mHSCs (Figs. 5C and D). 18β-GA (80 μM) also slightly down-regulated the expression of PRDX2, but not PRDX1 in LX-2 cells (Fig. S10), and 18β-GA (20 and 40 μM) did not affect their expressions. PRDX1 and PRDX2 are members of the family of non-selenium peroxidases, which have similar structures and functions [34,35]. Therefore, PRDX1 was selected for subsequent experiments. 18β-GA significantly inhibited the enzymatic activity of recombinant human PRDX1 (rhPRDX1) through an H_2O_2 reduction assay (Fig. 5E). Furthermore, ROS levels, cell viability, and apoptosis were measured. The results showed that 18β-GA increased ROS levels, decreased cell viability, and promoted apoptosis of LX-2 cells. Interestingly, NAC (a ROS scavenger) alleviated the increase in ROS levels and the loss of cell viability induced by 18β-GA (Figs. 5F–H), suggesting that 18β-GA-induced ROS contributed to the induction of apoptosis. Collectively, these results revealed that 18β-GA effectively inhibited the catalytic activity of PRDX1 to induce ROS-mediated apoptosis.

3.6. Active cysteines of PRDX1 and PRDX2 were binding sites for 18β-GA

Next, the molecular mechanism of 18β-GA binding to PRDX1 and PRDX2 was explored. rhPRDX1 and rhPRDX2 were treated with P1, followed by conjugation with a fluorescent dye. The results showed that rhPRDX1 and rhPRDX2 were labeled with the probe (Figs. 6A and S11A). Furthermore, rhPRDX1 incubated with P1 was pretreated with 18β-GA or iodoacetamide (IAA). Fluorescence intensity indicated that P1 was weaker after pretreatment with 18β-GA or IAA, suggesting that 18β-GA potentially bound to the cysteine residues of PRDX1 (Fig. 6B). To further confirm that the Cys52 residue of PRDX1 is a direct binding site for 18β-GA, site-directed mutagenesis (Cys52Ser) was performed on the cysteine residue of PRDX1. The results confirmed that 18β-GA mainly covalently modified Cys52 in PRDX1 (Fig. 6D). Thus, molecular docking analyses were performed between 18β-GA, PRDX1, and PRDX2. The results suggested that the cysteine binding sites were Cys52 of PRDX1 or Cys172 of PRDX2 (Figs. 6C, S11B, and S11C). Based on the above results, a possible binding mechanism reaction diagram was drawn (Fig. 6E).

3.7. Silencing of PRDX1 aggravated ROS production and induces apoptosis

To further verify that 18β-GA targeting *PRDX1* induced apoptosis to exert an anti-fibrotic function, knockdown of *PRDX1* by siRNA was conducted in LX-2 cells. The results indicate that silencing of *PRDX1* resulted in lower expression levels of PRDX1 (Figs. 7A and B).

Interestingly, silencing of *PRDX1* with or without 18β-GA increased the production of ROS, induced apoptosis by releasing Cyt C, and alleviated hepatic fibrosis (Figs. 7C and D). In addition, *PRDX1* silencing reduced COL1α1 and α-SMA protein levels (Fig. 7C). Flow cytometry analysis indicated that *PRDX1* knockdown contributed to the apoptosis of LX-2 cells (Fig. 7E). Collectively, these results revealed that silencing of *PRDX1* aggravated ROS production, induced apoptosis, and alleviated hepatic fibrosis.

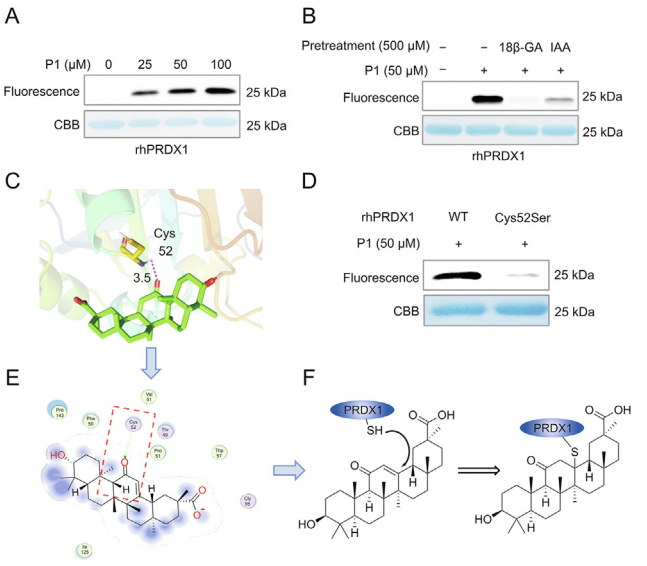

Fig. 6. 18β-GA bound to the cysteine residue of PRDX1. (A) P1 labeling of rhPRDX1. (B) Competition of P1 labeling of rhPRDX1 with or without 18β-GA or a cysteine-alkylating agent iodoacetamide (IAA). (C) A binding model of 18β-GA with PRDX1 generated by molecular docking. (D) The labeling of rhPRDX1 and its Cys52Ser mutant with P1. (E) Binding mechanism diagram between 18β-GA and PRDX1. WT: wild type.

4. Discussion

In the present study, it was confirmed that the natural compound 18β-GA had a strong inhibitory activity against hepatic fibrosis in both BDL-induced mice and activated-HSC (mHSCs and LX-2 cells). Through chemical biology studies, the target proteins of 18β-GA were identified using ABPP. Further research showed that 18β-GA targeted PRDX1 and PRDX2 and bound to cysteine residues to suppress antioxidant activities, resulting in the accumulation of cellular ROS to promote apoptosis and ameliorate hepatic fibrosis (Scheme 2). Thus, the data revealed the direct target proteins and exact mechanisms of 18β-GA in ameliorating hepatic fibrosis.

Liver disease is one of the most important factors affecting morbidity and mortality worldwide, leading to serious public health problems. Every year, approximately 2 million people worldwide die from liver diseases [36,37]. Hepatic fibrosis is a pathological process that refers to the abnormal deposition of ECM resulting from various pathogenic factors, which leads to various liver diseases, such as liver hepatitis, cirrhosis, and liver cancer. Thus, prevention and treatment of hepatic fibrosis are urgently needed [38,39]. Natural products that effectively inhibit hepatic fibrosis are significant for the development of promising treatments for liver diseases [40–43]. 18β-GA is a potent biologically active compound for the treatment of multiple liver diseases through its anti-inflammatory and anti-allergic effects [44,45]. The specific molecular mechanism and target proteins of 18β-GA require further investigation.

The target proteins of 18β-GA were identified using ABPP. In recent years, direct target proteins of several important natural products have been identified, including andrographolide [46], artemisinin [47,48], and curcumin [49]. The data from the current study indicated that 18β-GA could target PRDX1 or PRDX2

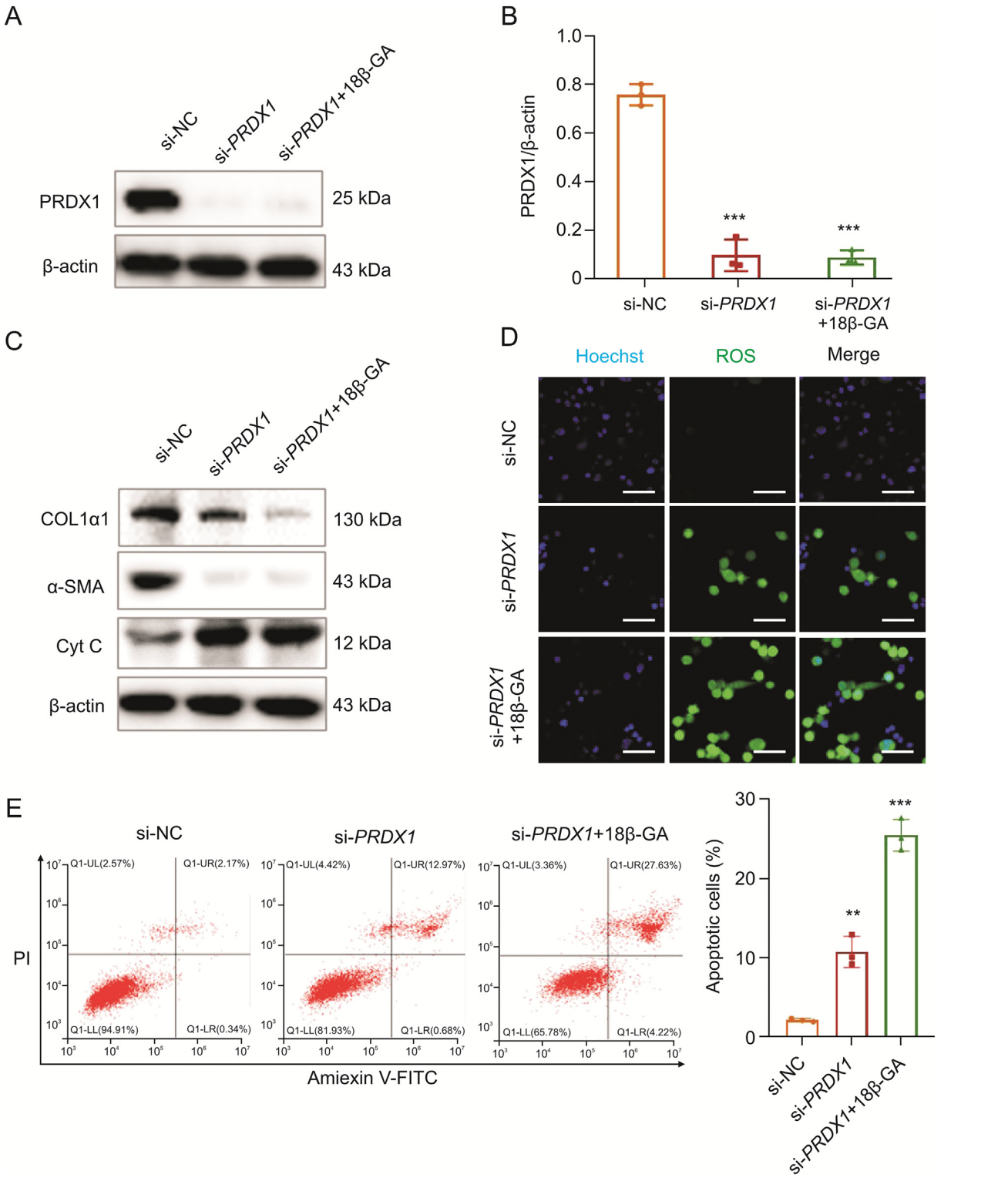

Fig. 7. Silencing of *PRDX1* accelerated hepatic fibrosis. (A) PRDX1 expression in LX-2 cells treated with si-*PRDX1* or 18β-GA (40 μM) incubation. (B) Densitometry analysis of protein levels in the Western blot corresponding to Fig. 7A ($n = 3$). (C) LX-2 cells infected with si-*PRDX1* were blotted for COL1α1, α-SMA, and Cyt C. (D) Intracellular ROS (green) staining after transfection with si-*PRDX1*, scale bar = 50 μm. (E) A cell death assay with si-*PRDX1* to monitor apoptotic cells by flow cytometry in LX-2 cells ($n = 3$). Mean ± SEM, $^{*}P < 0.01$, $^{**}P < 0.001$ vs. si-negative control (NC) group.

proteins and bind to cysteine residues to suppress its antioxidant activity. Targeting PRDX1 and PRDX2 to mediate ROS-induced apoptosis in cancer cells has been reported previously [32]. Interestingly, it was also confirmed that 18β-GA targeting PRDX1 and PRDX2 resulted in the accumulation of cellular ROS to further promote apoptosis in activated HSCs; thus, 18β-GA ameliorated hepatic fibrosis. Notably, PRDX1 and PRDX2 belong to the peroxiredoxin (PRDX) family, a class of catalytic enzymes in the antioxidant system [50]. PRDX1 and PRDX2 also protect against oxidative stress by inhibiting ROS-dependent signaling pathways

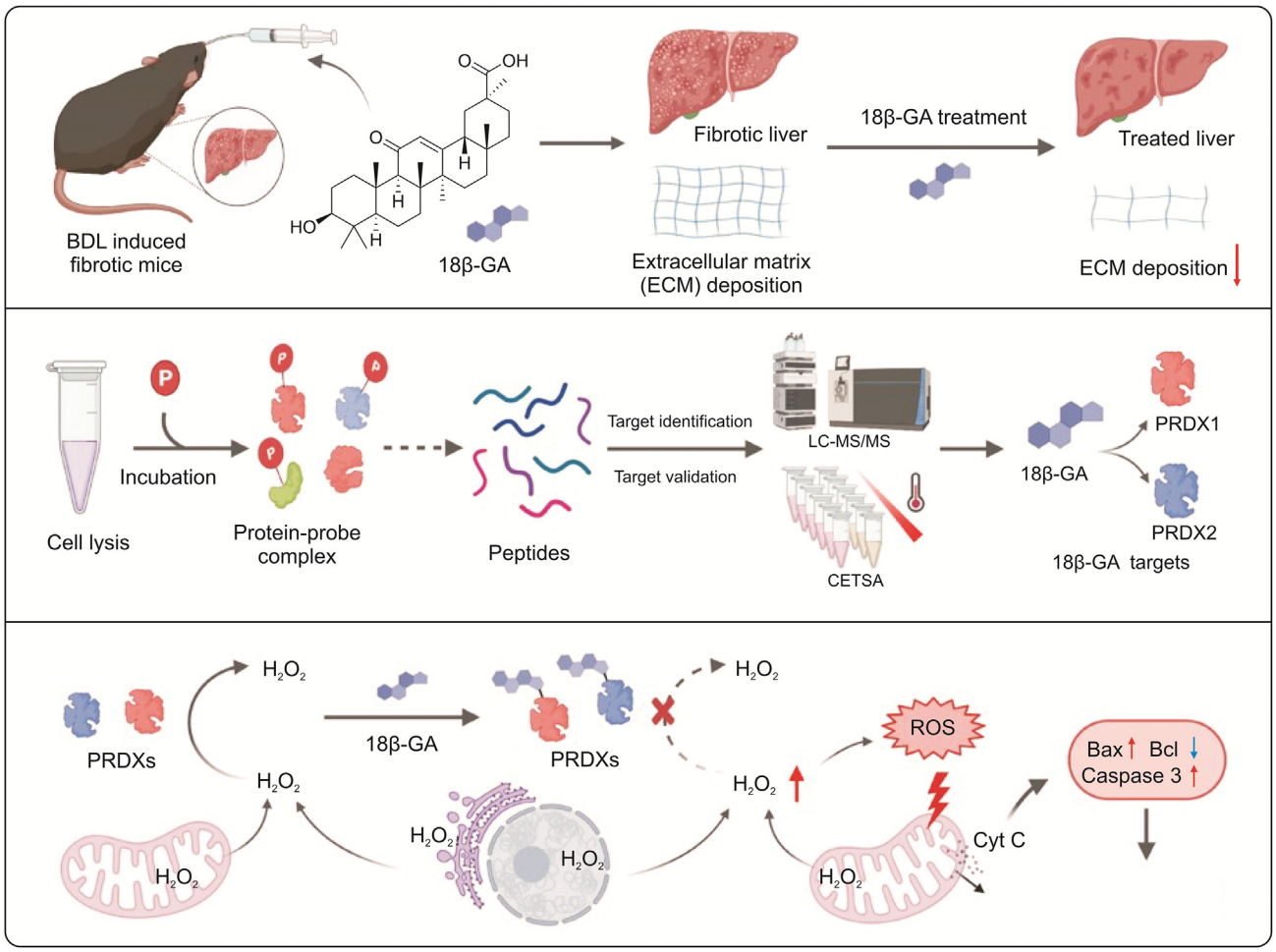

Scheme 2. Schematic summary of the study. 18β-GA ameliorated BDL-induced hepatic fibrosis. ABPP combined with CETSA strategy revealed that 18β-GA directly targeted PRDX1 and PRDX2. 18β-GA induced ROS-mediated apoptosis in activated-HSC via regulating PRDXs.

[51,52]. ROS play critical roles in mediating major pathways of cell signaling and apoptosis [53,54]. ROS such as O^{2-} and H_2O_2 lead to oxidative stress, which causes cell apoptosis [55]. PRDX2 has been previously suggested as a potential biomarker for hepatitis B virus-related hepatic fibrosis for early diagnosis [56]. Furthermore, other proteins in the PRDX family also play crucial roles in mediating oxidative stress in nonalcoholic steatohepatitis and cholestatic liver injury [57,58].

In the present study, it was found that 18β-GA effectively inhibited PRDX1 catalytic activity without affecting its protein expression. Inhibition of PRDX1 by 18β-GA further increased ROS levels and induced activated-HSC apoptosis, and these effects were rescued by the antioxidant NAC, which is the further evidence of 18β-GA-induced apoptosis by ROS. Importantly, previous research revealed that PRDXs can be reduced by peroxides to sulfenic acid by catalyzing the oxidation of cysteine [59]. Notably, both PRDX1 (Cys173 or Cys52) and PRDX2 (Cys172 or Cys51) are required to complete the peroxidative cycle [26,60]. The data demonstrated that 18β-GA covalently bound to Cys52 of PRDX1 and Cys172 of PRDX2, impairing their peroxidative cycle and inhibiting their antioxidant activities. This result is consistent with previous reports [61–63]. Silencing PRDX1 aggravates ROS production, induces apoptosis, and alleviates hepatic fibrosis.

In addition to PRDX1 and PRDX2, 18β-GA may also ameliorate hepatic fibrosis by targeting other proteins, as the results showed that 18β-GA targeted the voltage-dependent anion channel (VDAC). The VDAC is situated across the outer membrane of mitochondria and facilitates the transport of ions and metabolites [64]. They are also regulatory factors for mitochondrial function and mitochondria-mediated apoptosis [65]. The acquired data also showed that 18β-GA impaired mitochondrial homeostasis, leading to the release of Cyt C and the apoptosis of activated-HSC, as evidenced by 18β-GA treatment decreasing the Bcl-2/Bax ratio and caspase activation. These potential target proteins of 18β-GA in hepatic fibrosis and other diseases warrant further studies.

5. Conclusions

Overall, the results of the present study showed that 18β-GA directly bound to PRDX1 and PRDX2 and inhibited their antioxidant activities. This further resulted in the elevation of cellular ROS levels, which induced apoptosis in activated HSCs. Thus, the data indicated the direct target proteins and exact mechanisms of 18β-GA for ameliorating hepatic fibrosis. In summary, 18β-GA induced ROS-mediated apoptosis to attenuate hepatic fibrosis by targeting the active cysteines of PRDX1 and PRDX2 in activated HSCs. These findings provide strong evidence for the further development of 18β-GA as a novel and promising therapeutic drug for the treatment of hepatic fibrosis.

CRediT author statement

Qian Zhang and **Piao Luo**: Project administration, Methodology, Validation, Investigation, Writing - Original draft preparation; **Liuhai Zheng**: Investigation, Software, Writing - Original draft preparation; **Jiayun Chen**: Investigation, Formal analysis; **Junzhe Zhang** and **Huan Tang**: Validation, Data curation; **Dandan Liu** and **Xueling He**: Investigation, Writing - Reviewing and Editing; **Qiaoli Shi**, **Liwei Gu**, **Jiahao Li** and **Qiuyan Guo**: Investigation; **Chuanbin Yang** and **Yin Kwan Wong:** Writing - Reviewing and Editing; **Fei Xia** and **Jigang Wang**: Conceptualization, Supervision, Resources, Project administration.

Declaration of competing interest

The authors declare that there are no conflicts of interest.

Acknowledgments

The authors gratefully acknowledge the financial support from the Innovation Team and Talents Cultivation Program of the National Administration of Traditional Chinese Medicine, China (Grant No.: ZYYCXTD-C-202002), the National Key Research and Development Program of China, China (Grant No.: 2020YFA0908000), the National Natural Science Foundation of China, China (Grant Nos.: 81803389, 81903588, 32101219, 81702580, 82074098, 81903866, and 81803456), and the Fundamental Research Funds for the Central Public Welfare Research Institutes, China (Grant Nos.: ZZ14-YQ-050, ZZ14-YQ-059, ZZ15-ND-10, ZZ15-YQ-063, ZZ14-ND-010, and ZZ14-FL-002).

Appendix A. Supplementary data

Supplementary data to this article can be found online at https://doi.org/10.1016/j.jpha.2022.06.001.

References

[1] M.M. Aydın, K.C. Akçalı, Liver fibrosis, Turk. J. Gastroenterol. 29 (2018) 14–21.
[2] P. Ginès, A. Krag, J.G. Abraldes, et al., Liver cirrhosis, Lancet 398 (2021) 1359–1376.
[3] E. Seki, D.A. Brenner, Recent advancement of molecular mechanisms of liver fibrosis, J. Hepatobil. Pancreat. Sci. 22 (2015) 512–518.
[4] T. Higashi, S.L. Friedman, Y. Hoshida, Hepatic stellate cells as key target in liver fibrosis, Adv. Drug Deliv. Rev. 121 (2017) 27–42.
[5] T. Tsuchida, S.L. Friedman, Mechanisms of hepatic stellate cell activation, Nat. Rev. Gastroenterol. Hepatol. 14 (2017) 397–411.
[6] Y. Jia, F. Wang, Q. Guo, et al., Curcumol induces RIPK1/RIPK3 complex-dependent necroptosis via JNK1/2-ROS signaling in hepatic stellate cells, Redox Biol. 19 (2018) 375–387.
[7] Z. Zhang, Z. Yao, S. Zhao, et al., Interaction between autophagy and senescence is required for dihydroartemisinin to alleviate liver fibrosis, Cell Death Dis. 8 (2017), e2886.
[8] S. Bi, F. Chu, M. Wang, et al., Ligustrazine-oleanolic acid glycine derivative, G-TOA, selectively inhibited the proliferation and induced apoptosis of activated HSC-T6 cells, Molecules 21 (2016), 1599.
[9] B.N. Whitley, E.A. Engelhart, S. Hoppins, Mitochondrial dynamics and their potential as a therapeutic target, Mitochondrion 49 (2019) 269–283.
[10] G. Lenaz, The mitochondrial production of reactive oxygen species: Mechanism and implications in human pathology, IUBMB Life 52 (2001) 159–164.
[11] T. Luangmonkong, S. Suriguga, H.A.M. Mutsaers, et al., Targeting oxidative stress for the treatment of liver fibrosis, Rev. Physiol. Biochem. Pharmacol. 175 (2018) 71–102.
[12] S. Liang, T. Kisseleva, D.A. Brenner, The role of NADPH oxidases (NOXs) in liver fibrosis and the activation of myofibroblasts, Front. Physiol. 7 (2016), 17.
[13] H.J. Lin, C.P. Tseng, C.F. Lin, et al., A Chinese herbal decoction, modified Yi Guan Jian, induces apoptosis in hepatic stellate cells through an ROS-mediated mitochondrial/caspase pathway, Evid. Based Complem. Alternat. Med. 2011 (2011), 459531.
[14] A. Martí-Rodrigo, F. Alegre, Á.B. Moragrega, et al., Rilpivirine attenuates liver fibrosis through selective STAT1-mediated apoptosis in hepatic stellate cells, Gut 69 (2020) 920–932.
[15] H. Zheng, X. Wang, Y. Zhang, et al., Pien-Tze-Huang ameliorates hepatic fibrosis via suppressing NF-κB pathway and promoting HSC apoptosis, J. Ethnopharmacol. 244 (2019), 111856.
[16] D. Meng, Z. Li, G. Wang, et al., Carvedilol attenuates liver fibrosis by suppressing autophagy and promoting apoptosis in hepatic stellate cells, Biomed. Pharmacother. 108 (2018) 1617–1627.
[17] C. Bailly, G. Vergoten, Glycyrrhizin: An alternative drug for the treatment of COVID-19 infection and the associated respiratory syndrome? Pharmacol. Ther. 214 (2020), 107618.
[18] L. Wang, R. Yang, B. Yuan, et al., The antiviral and antimicrobial activities of licorice, a widely-used Chinese herb, Acta Pharm. Sin. B 5 (2015) 310–315.
[19] Y.-H. Luo, C. Wang, W.-T. Xu, et al., 18β-glycyrrhetinic acid has Anti-cancer effects via inducing apoptosis and G2/M cell cycle arrest, and inhibiting migration of A549 lung cancer cells, OncoTargets Ther. 14 (2021) 5131–5144.
[20] A. Roohbakhsh, M. Iranshahy, M. Iranshahi, Glycyrrhetinic acid and its derivatives: Anti-cancer and cancer chemopreventive properties, mechanisms of action and structure-cytotoxic activity relationship, Curr. Med. Chem. 23 (2016) 498–517.
[21] X. Tian, Y. Liu, X. Liu, et al., Glycyrrhizic acid ammonium salt alleviates Concanavalin A-induced immunological liver injury in mice through the regulation of the balance of immune cells and the inhibition of hepatocyte apoptosis, Biomed. Pharmacother. 120 (2019), 109481.
[22] X. Huo, X. Meng, J. Zhang, et al., Hepatoprotective effect of different combinations of 18α- and 18β-Glycyrrhizic acid against CCl_4-induced liver injury in rats, Biomed. Pharmacother. 122 (2020), 109354.
[23] J.-Y. Li, H.-Y. Cao, P. Liu, Glycyrrhizic acid in the treatment of liver diseases: Literature review, BioMed Res. Int. 2014 (2014), 872139.
[24] C.G. Tag, S. Sauer-Lehnen, S. Weiskirchen, et al., Bile duct ligation in mice: Induction of inflammatory liver injury and fibrosis by obstructive cholestasis, J. Vis. Exp. (2015), 52438.
[25] N. Liu, J. Feng, X. Lu, et al., Isorhamnetin inhibits liver fibrosis by reducing autophagy and inhibiting extracellular matrix formation via the TGF-β1/Smad3 and TGF-β1/p38 MAPK Pathways, Mediat. Inflamm. 2019 (2019), 6175091.
[26] Y. Sun, Y. Qiao, Y. Liu, et al., *ent*-Kaurane diterpenoids induce apoptosis and ferroptosis through targeting redox resetting to overcome cisplatin resistance, Redox Biol. 43 (2021), 101977.
[27] X. Chen, W. Li, C. Xu, et al., Comparative profiling of analog targets: A case study on resveratrol for mouse melanoma metastasis suppression, Theranostics 8 (2018) 3504–3516.
[28] P. Luo, D. Liu, Q. Zhang, et al., Celastrol induces ferroptosis in activated HSCs to ameliorate hepatic fibrosis via targeting peroxiredoxins and HO-1, Acta Pharm. Sin. B 12 (2022) 2300–2314.
[29] Y.T. Lim, N. Prabhu, L. Dai, et al., An efficient proteome-wide strategy for discovery and characterization of cellular nucleotide-protein interactions, PLoS One 13 (2018), e0208273.
[30] Y. Huang, S.-H. Yu, W.-X. Zhen, et al., Tanshinone I, a new EZH2 inhibitor restricts normal and malignant hematopoiesis through upregulation of *MMP9* and *ABCG2*, Theranostics 11 (2021) 6891–6904.
[31] C.-X. Liu, Q.-Q. Yin, H.-C. Zhou, et al., Adenanthin targets peroxiredoxin I and II to induce differentiation of leukemic cells, Nat. Chem. Biol. 8 (2012) 486–493.
[32] X. Chen, Y. Zhao, W. Luo, et al., Celastrol induces ROS-mediated apoptosis via directly targeting peroxiredoxin-2 in gastric cancer cells, Theranostics 10 (2020) 10290–10308.
[33] D. Martinez Molina, R. Jafari, M. Ignatushchenko, et al., Monitoring drug target engagement in cells and tissues using the cellular thermal shift assay, Science 341 (2013) 84–87.
[34] S.G. Rhee, S.W. Kang, T.S. Chang, et al., Peroxiredoxin, a novel family of peroxidases, IUBMB Life 52 (2001) 35–41.
[35] S.G. Rhee, H.Z. Chae, K. Kim, Peroxiredoxins: A historical overview and speculative preview of novel mechanisms and emerging concepts in cell signaling, Free Radic. Biol. Med. 38 (2005) 1543–1552.
[36] S.K. Asrani, H. Devarbhavi, J. Eaton, et al., Burden of liver diseases in the world, J. Hepatol. 70 (2019) 151–171.
[37] F.-S. Wang, J.-G. Fan, Z. Zhang, et al., The global burden of liver disease: The major impact of China, Hepatology 60 (2014) 2099–2108.
[38] C. Peng, A.G. Stewart, O.L. Woodman, et al., Non-alcoholic steatohepatitis: A review of its mechanism, models and medical treatments, Front. Pharmacol. 11 (2020), 603926.
[39] R.J. Chen, H.H. Wu, Y.J. Wang, Strategies to prevent and reverse liver fibrosis in humans and laboratory animals, Arch. Toxicol. 89 (2015) 1727–1750.
[40] X. Ma, Y. Jiang, J. Wen, et al., A comprehensive review of natural products to fight liver fibrosis: Alkaloids, terpenoids, glycosides, coumarins and other compounds, Eur. J. Pharmacol. 888 (2020), 173578.
[41] L. Shan, Z. Liu, L. Ci, et al., Research progress on the anti-hepatic fibrosis action and mechanism of natural products, Int. Immunopharmacol. 75 (2019), 105765.
[42] K.K. Wai, Y. Liang, L. Zhou, et al., The protective effects of *Acanthus ilicifolius* alkaloid A and its derivatives on pro- and anti-inflammatory cytokines in rats with hepatic fibrosis, Biotechnol. Appl. Biochem. 62 (2015) 537–546.
[43] H. Wang, Y. Zhang, R. Bai, et al., Baicalin attenuates alcoholic liver injury through modulation of hepatic oxidative stress, inflammation and sonic hedgehog pathway in rats, Cell. Physiol. Biochem. 39 (2016) 1129–1140.
[44] S.Y. Wu, W.J. Wang, J.H. Dou, et al., Research progress on the protective effects of licorice-derived 18β-glycyrrhetinic acid against liver injury, Acta Pharmacol. Sin. 42 (2021) 18–26.
[45] X. Li, R. Sun, R. Liu, Natural products in licorice for the therapy of liver

diseases: Progress and future opportunities, Pharmacol. Res. 144 (2019) 210–226.
[46] J. Wang, X.F. Tan, V.S. Nguyen, et al., A quantitative chemical proteomics approach to profile the specific cellular targets of andrographolide, a promising anticancer agent that suppresses tumor metastasis, Mol. Cell. Proteomics 13 (2014) 876–886.
[47] J. Zhang, X. Sun, L. Wang, et al., Artesunate-induced mitophagy alters cellular redox status, Redox Biol. 19 (2018) 263–273.
[48] J. Wang, C.J. Zhang, W.N. Chia, et al., Haem-activated promiscuous targeting of artemisinin in Plasmodium falciparum, Nat. Commun. 6 (2015), 10111.
[49] J. Wang, J. Zhang, C.J. Zhang, et al., *In situ* proteomic profiling of curcumin targets in HCT116 colon cancer cell line, Sci. Rep. 6 (2016), 22146.
[50] B. Knoops, V. Argyropoulou, S. Becker, et al., Multiple roles of peroxiredoxins in inflammation, Mol. Cell. 39 (2016) 60–64.
[51] C. Ding, X. Fan, G. Wu, Peroxiredoxin 1 - an antioxidant enzyme in cancer, J. Cell Mol. Med. 21 (2017) 193–202.
[52] S. Wang, Z. Chen, S. Zhu, et al., PRDX2 protects against oxidative stress induced by H. pylori and promotes resistance to cisplatin in gastric cancer, Redox Biol. 28 (2020), 101319.
[53] Z. Zou, H. Chang, H. Li, et al., Induction of reactive oxygen species: An emerging approach for cancer therapy, Apoptosis 22 (2017) 1321–1335.
[54] D.B. Zorov, M. Juhaszova, S.J. Sollott, Mitochondrial reactive oxygen species (ROS) and ROS-induced ROS release, Physiol. Rev. 94 (2014) 909–950.
[55] K. Pant, A.K. Yadav, P. Gupta, et al., Butyrate induces ROS-mediated apoptosis by modulating miR-22/SIRT-1 pathway in hepatic cancer cells, Redox Biol. 12 (2017) 340–349.
[56] Y. Lu, J. Liu, C. Lin, et al., Peroxiredoxin 2: A potential biomarker for early diagnosis of hepatitis B virus related liver fibrosis identified by proteomic analysis of the plasma, BMC Gastroenterol. 10 (2010), 115.
[57] J. Zhang, X. Guo, T. Hamada, et al., Protective Effects of peroxiredoxin 4 (PRDX4) on cholestatic liver injury, Int. J. Mol. Sci. 19 (2018), 2509.
[58] M.H. Kim, J.B. Seong, J.W. Huh, et al., Peroxiredoxin 5 ameliorates obesity-induced non-alcoholic fatty liver disease through the regulation of oxidative stress and AMP-activated protein kinase signaling, Redox Biol. 28 (2020), 101315.
[59] B.L. Hopkins, M. Nadler, J.J. Skoko, et al., A peroxidase peroxiredoxin 1-specific redox regulation of the novel FOXO3 microRNA target let-7, Antioxid, Redox Signal 28 (2018) 62–77.
[60] Z.A. Wood, L.B. Poole, P.A. Karplus, Peroxiredoxin evolution and the regulation of hydrogen peroxide signaling, Science 300 (2003) 650–653.
[61] Q. Zhao, Y. Ding, Z. Deng, et al., Natural products triptolide, celastrol, and withaferin A inhibit the chaperone activity of peroxiredoxin I, Chem. Sci. 6 (2015) 4124–4130.
[62] Y. Zhang, C. Sun, G. Xiao, et al., *S*-nitrosylation of the peroxiredoxin-2 promotes *S*-nitrosoglutathione-mediated lung cancer cells apoptosis via AMPK-SIRT1 pathway, Cell Death Dis. 10 (2019), 329.
[63] B. Turner-Ivey, Y. Manevich, J. Schulte, et al., Role for Prdx1 as a specific sensor in redox-regulated senescence in breast cancer, Oncogene 32 (2013) 5302–5314.
[64] N.M. Mazure, VDAC in cancer, Biochim. Biophys. Acta Bioenerg. 1858 (2017) 665–673.
[65] V. Shoshan-Barmatz, V. De Pinto, M. Zweckstetter, et al., VDAC, a multifunctional mitochondrial protein regulating cell life and death, Mol. Aspect. Med. 31 (2010) 227–285.